

Electronic Supplementary Information

Solvent-modulated slow magnetic relaxation in a two-dimensional compound composed of cobalt(II) single-chain magnets

Yan-Qin Wang, Wei-Wei Sun, Zhen-Dong Wang, Qin-Xiang Jia, En-Qing Gao* and You Song

Synthesis: A mixture of $\text{CoCl}_2 \cdot 6\text{H}_2\text{O}$ (0.0476 g, 0.2 mmol), NaN_3 (0.026 g, 0.4 mmol), HL (0.0181 g, 0.1 mmol) was dissolved into ethanol (5 ml) and water (2 ml), then this solution was sealed in a Teflon-lined stainless steel vessel (25 ml), heated at 70 °C for 4 days under autogenous pressure. After cooling to room temperature, purple crystals of **1**·Co in a yield of 60% based on L and some pink powder were obtained. Our efforts to synthesize a pure sample of **1** were unsuccessful, but the pink powder could be removed by rinsing with ethanol. Anal. calcd. for $\text{C}_{16}\text{H}_{20}\text{Co}_3\text{N}_{14}\text{O}_{12}$: C, 24.73; H, 2.59; N, 25.23. Found: C, 24.42; H, 2.95; N, 25.74%. Main IR bands (KBr, cm^{-1}): 3548m, 3479m, 3399m, 2086vs, 2056vs, 1647s, 1629s, 1580w, 1386s, 1304w, 1214w, 740w. Upon heating at 100 °C the crystals of **1** collapsed and became opaque, and the colour changes from pink to blue-purple.

Crystal Data Collection and Refinement: Diffraction data for **1** was collected at 293 K on a Bruker Apex II CCD area detector equipped with graphite-monochromated Mo $K\alpha$ radiation ($\lambda = 0.71073 \text{ \AA}$). Empirical absorption corrections were applied using the SADABS program. The structures were solved by the direct method and refined by the full-matrix least-squares method on F^2 using the SHELXL program, with anisotropic displacement parameters for all non-hydrogen atoms. All the hydrogen atoms attached to carbon atoms were placed in calculated positions and refined using the riding model. The water hydrogen atoms attached to O5 and O6 were located from the difference Fourier map and refined with restrained O-H and H···H distances (6 restrains using the DFIX instruction).

Crystal data: $\text{C}_{16}\text{H}_{20}\text{Co}_3\text{N}_{14}\text{O}_{12}$, $M_r = 777.25$; Triclinic, $P\bar{1}$; $a = 8.527(1) \text{ \AA}$, $b = 8.921(2) \text{ \AA}$, $c = 10.157(1) \text{ \AA}$, $\alpha = 104.645(2)$, $\beta = 113.488(1)$, $\gamma = 94.976(2)$, $V = 670.18(9) \text{ \AA}^3$, $Z = 1$, $D_c =$

1.926 g/cm⁻³, $\mu(\text{Mo-K}\alpha) = 1.924 \text{ mm}^{-1}$, $T = 293(2) \text{ K}$, 2973 unique reflections with $R_{\text{int}} = 0.0200$, GOF on $F^2 = 0.999$, final $R_1 = 0.0401$ and $wR_2 = 0.0904$ for $I \geq 2\sigma(I)$, $R_1 = 0.0576$ and $wR_2 = 0.1005$ for all data.

Physical measurements: Elemental analyses (C, H, and N) were performed on a Perkin-Elmer 2400 CHN elemental analyzer. FT-IR spectra were recorded in the range 500-4000 cm⁻¹ on a Nicolet NEXUS 670 spectrophotometer using KBr pellets. Solid-state UV-visible reflectance spectra were recorded on Shimadzu UV-2400PC. TG analyses were carried out on a Mettler Toledo TGA/SDTA851 instrument under flowing air at a heating rate of 5 °C min⁻¹. Powder X-ray diffraction data were collected on a Bruker D8 ADVANCE diffractometer equipped with Cu K α at a scan speed of 1° min⁻¹. Magnetic measurements were performed on a Quantum Design MPMS XL5 SQUID magnetometer. The experimental susceptibilities were corrected for the diamagnetism of the constituent atoms (Pascal's tables). The dehydrated phase **2** is very sensitive to air and **1** is readily recovered by exposing **2** to air for seconds. Thus the magnetic measurements of **2** were performed using a sample sealed up in paraffin wax. The data for the sample were obtained by subtracting the diamagnetic contribution of paraffin wax, which was measured separately.

Magnetic susceptibility for Ising chains with alternating J_1 - J_1 - J_2 interactions. Based on the Hamiltonian

$$H = -J_1 \sum (S_{3i,z} S_{3i+1,z} + S_{3i+1,z} S_{3i+2,z}) - J_2 \sum (S_{3i-1,z} S_{3i,z}) \quad (1)$$

the parallel component of the magnetic susceptibility per Co₃ unit for the alternating system can be expressed as [see ref. 6d]

$$\chi_{\parallel} = \frac{N\beta^2 g^2}{4kT} \frac{9 \exp(J_1/2kT) + 2 \exp(-J_2/2kT) + \exp(-J_1/2kT)}{\exp(J_1/2kT - J_2/2kT) + \exp(-J_1/2kT - J_2/2kT) + 2} \quad (2)$$

To fit the experimental χ data for polycrystalline samples, the relationship $\chi = \chi_{\parallel}/3$ was applied (χ_{\perp} is much smaller than χ_{\parallel} for Ising chains).

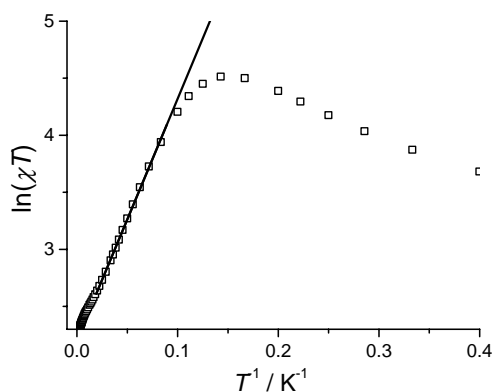


Fig. S1. The $\ln(\chi T)$ versus T^{-1} scaling plots for **1**. The solid line represents the best linear fit in the range 12-40 K. The low-temperature deviation from linearity may be due to a combination of the field effect, finite-chain effect and weak interchain AF interactions. The slope (21 K) of the linear regime is routinely related to Δ_{ξ} , the contribution of intrachain coupling to the total anisotropy energy. A quick comparison indicates $\Delta_{\tau} \approx 2\Delta_{\xi}$ ($\Delta_{\tau} = 41$ K according to the dynamic data), in good agreement with the Glauber dynamics for infinite Ising chains. But it is also possible that finite chains are relevant, with $\Delta_{\tau} = \Delta_{\xi} + \Delta_A$ (see ref. 4a), where Δ_A (the energy barrier of spin flip in absence of magnetic coupling) happens to be close to Δ_{ξ} .

NOTES: Owing to the comparable and alternating exchange pathways, there is no clear relationship between Δ_{ξ} and intrachain coupling J 's. The temperature dependence of χ [or $\ln(\chi T)$] is expressed by eqn. 2 (vide supra), so the linear $\ln(\chi T)$ - $1/T$ relationship, which is theoretically deduced for uniform chains (with one J or J_{eff} between nearest spins or effective spins, see refs. 4a, 4b), is only a rough approximation for our chain. This may be an important origin of the deviation observed here. Thus, the Δ_{ξ} value obtained is also a rough estimation. Even the relationships of Δ_{τ} , Δ_{ξ} and Δ_A , originally deduced for uniform chains, may do not hold exactly for the present system. So the above scaling treatment and sequent discussion, which seems to have become routine for SCMs, are only tentative here. The alternating systems need further investigation, especially in the theoretical aspects, although more complicated to solve [ref. 4b].

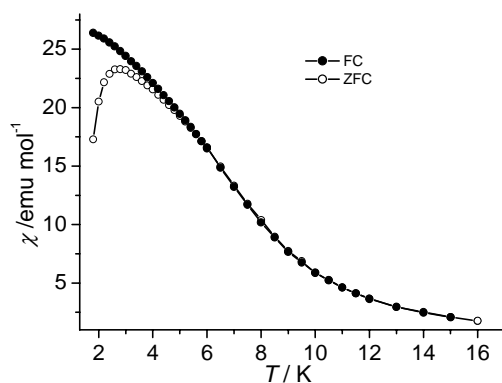


Fig. S2. ZFC and FC magnetization curves of **1** at 20 Oe.

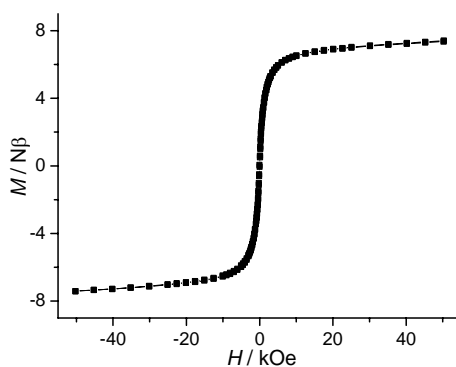


Fig. S3. Isothermal magnetization of **1** at 2 K.

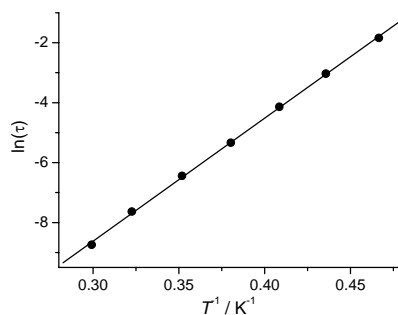


Fig. S4. The $\ln(\tau)$ versus $1/T$ plot of **1**, the solid line representing the fit to the Arrhenius law.

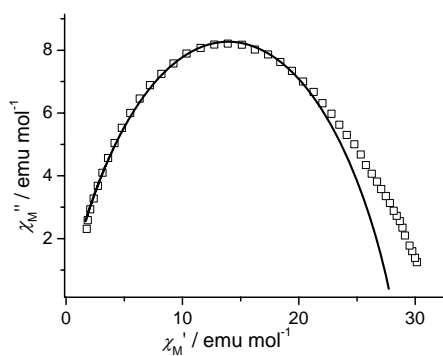


Fig. S5. Cole-Cole diagrams in the frequency range 1-1500 Hz with $H_{\text{dc}} = 0$, $H_{\text{ac}} = 3$ Oe for **1** (2.8 K).

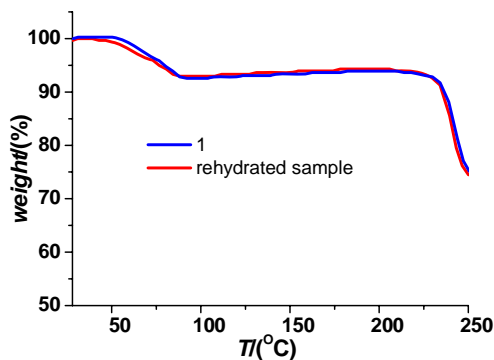


Fig. S6. The thermogravimetric curves of **1** and the rehydrated sample. The rehydrated sample was obtained by exposing **2** to air for 1 h. The two curves are almost superposed. The dehydration occurs in one step from around 50 to 100 °C with a weight loss of about 7.5%. This value is somewhat less than that (9.3%) expected from the crystallographic data, suggesting the partial loss of lattice water before the measurements. The framework decomposition occurs above 250 °C.

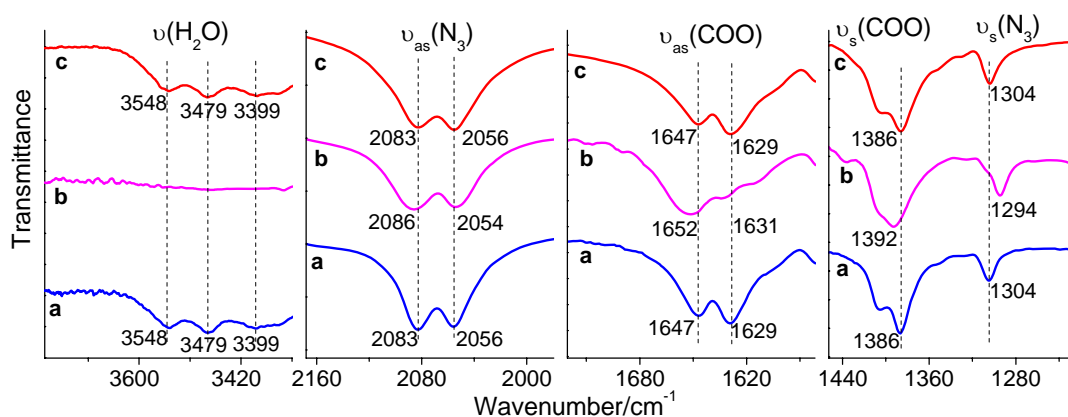


Fig. S7. The IR spectra of **1** (a), **2** (b) and the rehydrated sample (c). The spectrum of **2** was measured under vacuum. The disappearance of peaks at 3548, 3479, 3399 cm⁻¹ for **2** indicated the loss of water molecules. The changes in some of the main absorption bands are detectable for ν_{as}(N₃), ν_{as}(COO), ν_s(COO) and ν_s(N₃), suggesting the modification of the coordination of these groups, although it is difficult to get the information about the way how they changed. Moreover, the full recovery of the IR spectra after rehydration strongly supports that the transformation from **1** to **2** is reversible.

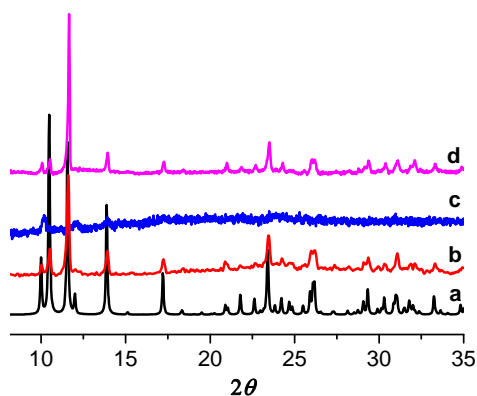


Fig. S8. Powder X-ray diffraction (PXRD) analyses: a) calculated from the crystallographic data of **1**; b) measured for **1**; c) measured for **2** (sealed in a glove-box); d) measured for the rehydrated sample. Apparently, **2** is a new phase with reduced crystallinity and can be recovered to **1**.

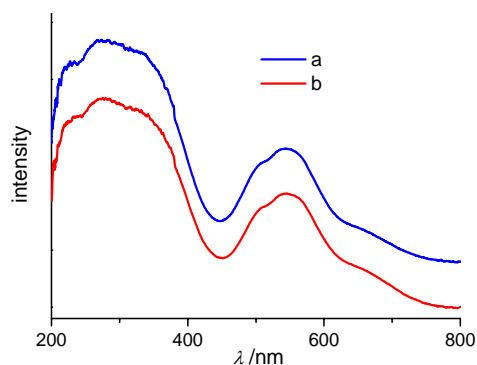


Fig. S9. Solid-state UV-vis spectra of **1** (a) and the rehydrated sample (b). The spectra features intense charge transfer absorption around 270 nm, and $d-d$ transition bands centered around 544 nm [${}^4T_{1g}(F) \rightarrow {}^4T_{1g}(P)$]. The shoulder at ca. 664 nm is assignable to ${}^4T_{1g}(F) \rightarrow {}^4A_{2g}$. The two spectra are essentially identical, demonstrating that the coordination environments of the metal ions is recovered upon rehydration.

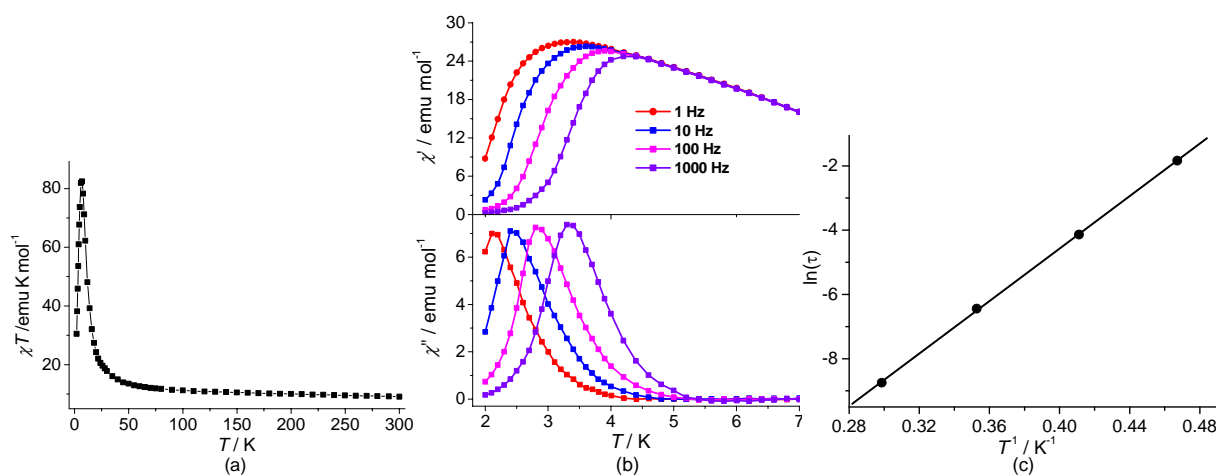


Fig. S10. Magnetic measurements for the rehydrated sample: **a)** χT vs T plot at 1 kOe; **b)** $\chi'(T)$ and $\chi''(T)$ plots with $H_{\text{dc}} = 0$ and $H_{\text{ac}} = 3.5$ Oe; **c)** The $\ln(\tau)$ versus $1/T$ plot, the solid line representing the fit to the Arrhenius law with $\tau_0 = 8.3 \times 10^{-10}$ s and $\Delta\tau = 40.8$ K. These magnetic measurements suggest the static and dynamic magnetic behaviours of **1** are recovered.

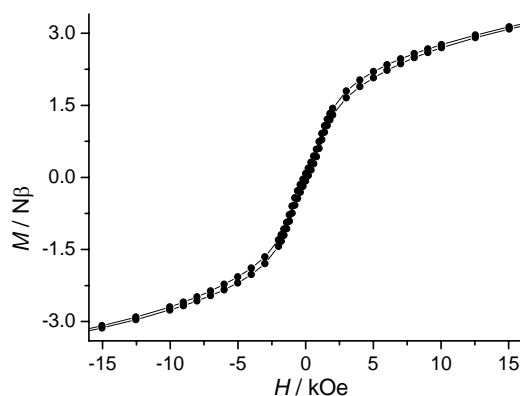


Fig. S11. The hysteresis loop of **2** at 2 K.

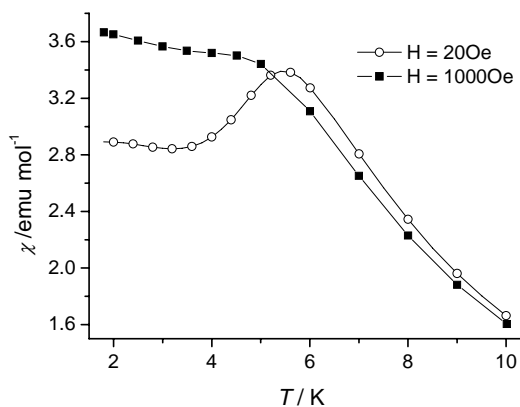


Fig. S12. Thermal magnetic susceptibility of **2** at 20 and 1000 Oe.

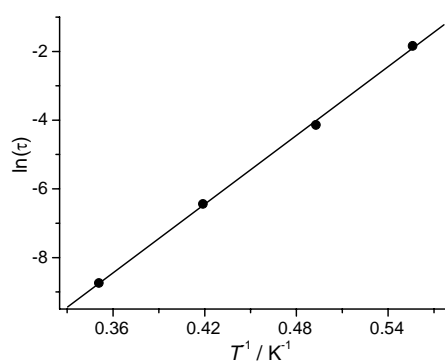


Fig. S13. The $\ln(\tau)$ versus $1/T$ plot of **2**, the solid line representing the fit to the Arrhenius law.

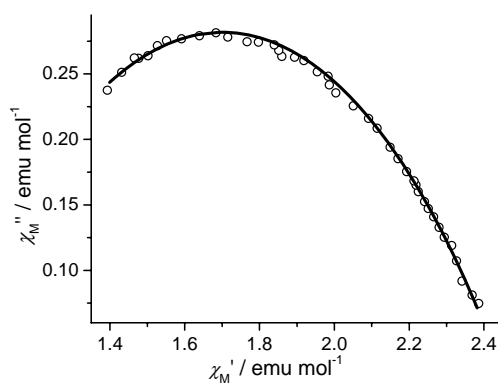


Fig. S14. Cole-Cole diagrams in the frequency range 1-1500 Hz with $H_{\text{dc}} = 0$, $H_{\text{ac}} = 3$ Oe for **2** (2.5 K).